Photothermal operation of high frequency nanoelectromechanical systems

A. Sampathkumar, T. W. Murray,[a] and K. L. Ekinci[b]
Aerospace and Mechanical Engineering Department, Boston University, Boston, Massachusetts 02215

(Received 27 December 2005; accepted 17 April 2006; published online 31 May 2006)

We describe photothermal operation of nanoelectromechanical systems (NEMS) in ambient atmosphere. Using a tightly focused modulated laser source, we have actuated the *out-of-plane* flexural resonances of *bilayered* doubly clamped beams. The optically detected displacement profiles in these beams are consistent with a model where the absorbed laser power results in a local temperature rise and a subsequent thermally induced bending moment. The described technique allows probing and actuation of NEMS with exquisite spatial and temporal resolution. From a device perspective, the technique offers immense frequency tunability and may enable future NEMS that can be remotely accessed without electronic coupling. © *2006 American Institute of Physics*. [DOI: 10.1063/1.2208381]

Nanoelectromechanical systems[1] (NEMS) are rapidly being developed for a variety of applications[2] as well as for exploring interesting regimes in fundamental physics.[3] In most of these endeavors, operation of a NEMS device involves actuating the device harmonically around its fundamental resonance and detecting the subsequent motion—while the device interacts with its environment.

The development of high precision motion transducers[4] at the nanoscale is key to realizing the full potential of NEMS. In particular, operation or mechanical testing of a NEMS device necessitates the local and precise application of a *harmonic* force to the nanomechanical element. To date, a variety of actuation methods with ultrahigh force and time resolution have been demonstrated, but obtaining nanoscale resolution in the position of the applied force still remains a significant challenge. In the magnetomotive[5] and electrostatic[6] NEMS actuation techniques, one generates a *uniform* harmonic force upon the actuation electrode which usually covers the nanomechanical element. Thus, using the aforementioned techniques, reliable operation in certain mechanical modes—e.g., the first harmonic mode of a nanomechanical doubly clamped beam—has not been possible. On the other hand, the AFM technique has enabled the application of forces to NEMS with high position accuracy, albeit with insufficient time resolution.[7]

Optical techniques have been used to probe micro-[8] and nanoscale[9] mechanical systems and biological systems.[10] In this letter, we use photothermal excitation to realize nanomechanical probing and actuation in the NEMS domain. We demonstrate high spatial and temporal resolutions by actuating the fundamental and the first harmonic resonant modes of a doubly clamped nanomechanical beam. The analysis presented captures the essentials of our experiments and offers insight into the ultimate limits of this technique.

The NEMS used in these experiments were Cr coated Si doubly clamped beams fabricated using standard techniques.[6] The measurements were performed in ambient atmosphere using the photoacoustic microscopy system depicted in Fig. 1(a).[11] The beams were excited using an electroabsorptive intensity modulated diode laser operating at a wavelength $\lambda=1550$ nm. The excitation power was of the form $P=P_0(1+\cos\omega\tau)$, where P_0 is the peak power level, ω is the modulation frequency, and τ is the time. The resulting displacement was detected using a path-stabilized Michelson interferometer utilizing a frequency doubled Nd:YAG (neodymium doped yttrium aluminum garnet) laser source ($\lambda=532$ nm). The excitation and detection probes passed through a single long working distance microscope objective with a numerical aperture of 0.40. We performed phase sensitive detection at ω using a rf lock-in amplifier. The minimum detectable displacement in our optical detection system was ~0.4 pm for the 0.7 Hz measurement bandwidth used. A piezodriven sample translation stage allowed high precision positioning of the optical spot upon the device.

We first probed the high frequency resonant modes of the NEMS beams. The beams had the following dimensions [$l\times w\times t$, see Fig. 1(a)]: $4<l<10$ μm, 250 nm$<w<1$ μm, and a total thickness $t=250$ nm comprising layers of Si ($t_{Si}=200$ nm) and Cr ($t_{Cr}=50$ nm). In Figs. 1(b) and 1(c), we display the measured fundamental and first harmonic modes of a 6 μm$\times$1 μm$\times$250 nm ($l\times w\times t$) beam. The excitation and detection powers, measured at the focal plane of the objective, were 2 and 0.20 mW, respectively. In the measurements, both the excitation and the detection spots were placed upon a set position on the beam and the harmonic beam displacement was recorded as a function of ω, as ω was swept around the resonance frequency. The optical spot was then moved to a different location and the measurement was repeated. At each measurement location, a Lorentzian displacement amplitude response curve as a function of ω was obtained, indicating that the resonator was operated within its linear regime. Representative displacement response curves are shown in the insets of both Figs. 1(b) and 1(c). The resonance peaks of the first two modes are at $\Omega_1/2\pi=18.9$ MHz and $\Omega_2/2\pi=59.2$ MHz. Such sets of rms displacement measurements as a function of spot position upon the NEMS resulted in the data in Figs. 1(b) and 1(c). The dashed lines in the plots are results from our numerical analyses (see discussion below). Note the general agreement. We suspect that the clamp motion [Fig. 1(b)] is due to the ~1 μm undercut in the structures. The Q factors obtained in these modes are $Q_1\approx30$ and $Q_2\approx54$, consistent with atmospheric damping.[12]

[a]Electronic mail: twmurray@bu.edu
[b]Electronic mail: ekinci@bu.edu

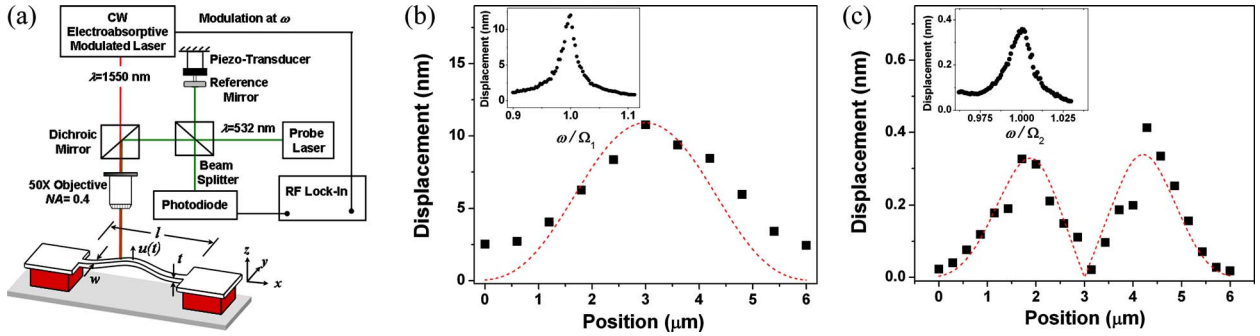

FIG. 1. (Color online) (a) Schematic diagram of the photothermal measurement setup. The rms displacement at the (b) fundamental mode and (c) first harmonic mode as a function of the optical spot position upon the beam. The dashed lines are results from detailed numerical analyses. The insets in both (b) and (c) show the resonance line shapes measured at points of maximum displacement, i.e., at (b) $x=l/2$ and (c) $x=3l/4$.

In a second set of measurements, we investigated the effect of incident excitation laser power P_0 on the rms displacement amplitude and Ω_1. Here, the optical spot was placed in the center of the beam and P_0 was increased incrementally. The results of these measurements on a 6 μm $\times$750 nm$\times$250 nm ($l\times w\times t$) beam are shown in Figs. 2(a) and 2(b). Figure 2(a) shows that the rms displacement amplitude is a highly *nonlinear* function of the excitation power. This is especially noticeable for power greater than 1 mW. The inset of Fig. 2(a) shows typical Lorentzian resonance line shapes at several values of P_0. The inset data indicate that the resonator itself is operating *linearly* as a damped harmonic system regardless of the drive power level. The threshold power for irreversible damage to the beams typically fell between 2 and 3 mW. In Fig. 2(b), the change in Ω_1 as a function of P_0 is shown. The drop in Ω_1 is quite remarkable, going from approximately 23.7 MHz at an excitation power of 0.23 mW to 12.8 MHz at 1.90 mW. We did not observe an appreciable change in Q with P_0. We note that the general trends in Figs. 2(a) and 2(b) were observed in all samples—albeit with some fluctuations in the magnitude of the effects. Nevertheless, the immense resonance frequency tunability available by this technique may be of importance for numerous NEMS applications.

We now turn to an analysis of photothermal NEMS operation. The temperature profile $T(x,\tau)$ in the beam can be approximated using the one-dimensional heat equation:

$$\frac{\partial^2 T(x,\tau)}{\partial x^2}+\frac{1}{\kappa}g(x,\tau)=\frac{1}{\eta}\frac{\partial T(x,\tau)}{\partial \tau}. \tag{1}$$

Here, κ and η are the thermal conductivity and diffusivity of the material, respectively. In this *dynamic* analysis, we shall only consider the heat source $g(x,\tau)$ due to the harmonically modulated portion of the laser $P_0\cos\omega\tau$. The dc portion of the source term will generate a corresponding *average* temperature rise of the beams, but not a modulation in temperature. We model $g(x,\tau)$ as a Gaussian centered at $x=x_0$ with a width of $2r_0$: $g(x,\tau)=(\Lambda P_A/\sqrt{\pi}r_0 wt)e^{-(x-x_0)^2/r_0^2}\cos\omega\tau$. The quantity Λ is the absorptivity of the medium and ΛP_A gives the total power absorbed by the medium.

The temperature distribution, in turn, generates a differential thermal expansion between the silicon beam and the Cr metallization layer—resulting in a harmonic stress component $\sigma_{xx}(x,z,\tau)$. The net effect is a bending moment $M_y(x,\tau)$ given by

$$M_y(x,\tau)=\int \sigma_{xx}(x,z,\tau)(z-z_n)w dz, \tag{2}$$

where the integral is over the yz cross section of the beam [see the coordinate system in Fig. 1(a)] and z_n denotes the coordinate of the neutral plane in the composite structure.[13] We can obtain an expression for $M_y(x,\tau)$ in terms of the temperature profile, the thicknesses t, thermal expansion coefficients α, and the moduli E of the Si and Cr layers as

$$M_y(x,\tau)=(\alpha_{\mathrm{Si}}-\alpha_{\mathrm{Cr}})\frac{wt_{\mathrm{Si}}t_{\mathrm{Cr}}(t_{\mathrm{Si}}+t_{\mathrm{Cr}})E_{\mathrm{Si}}E_{\mathrm{Cr}}}{2(E_{\mathrm{Si}}t_{\mathrm{Si}}+E_{\mathrm{Cr}}t_{\mathrm{Cr}})^2}$$
$$\times(E_{\mathrm{Si}}t_{\mathrm{Si}}-E_{\mathrm{Cr}}t_{\mathrm{Cr}})T(x,\tau). \tag{3}$$

In the presence of a harmonic bending moment, it can be shown that the flexural displacement $\mathcal{U}_z$ of a thin beam is described by[14]

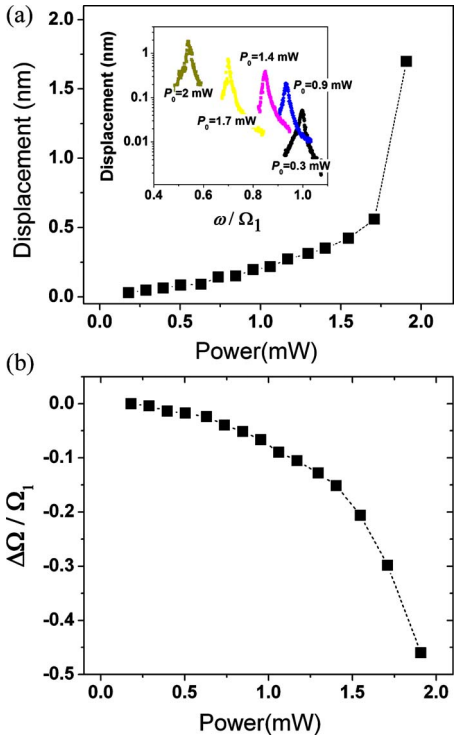

FIG. 2. (Color online) (a) The displacement and (b) the frequency shift as functions of excitation power in the fundamental mode. The inset in (a) shows the measured resonance line shapes at the indicated power value.

$$\rho A \frac{\partial^2 \mathcal{U}_z}{\partial \tau^2} + EI \frac{\partial^4 \mathcal{U}_z}{\partial x^4} = \frac{\partial^2 M_y}{\partial x^2}. \tag{4}$$

The linear mass density ρA and the flexural rigidity EI of the composite beam are determined in terms of the layer thicknesses and material properties.[15] In the vicinity of the nth mode, $\omega \approx \Omega_n$, $\mathcal{U}_z(x,\tau)$ can be expressed in terms of the eigenfunctions $\psi_n(x)$ of the unforced beam equation:[13]

$$\mathcal{U}_z(x,\tau) = \frac{1}{Ml^2} \frac{\psi_n(x)}{{\Omega_n}^2 - \omega^2 - i{\Omega_n}^2/Q_n} \times \int_0^l \psi_n(x') \frac{\partial^2 M_y(x',\tau)}{\partial {x'}^2} dx'. \tag{5}$$

Here, Ω_n is the mode frequency and Q_n is the mode quality factor.

In our numerical analyses, we first determined the temperature profile $T(x,\tau)$ by convolving the Green's function for Eq. (1) in an infinite one-dimensional medium[16] with $g(x,\tau)$, thus neglecting any reflections of thermal waves from the boundaries. The next step was determining the displacement $\mathcal{U}_z(x,\tau)$ through Eqs. (3) and (5). In our experiments, the probing and excitation points are identical, i.e., $x=x_0$. The measurement region is distributed over the detection spot size ($\sim$660 nm). Hence, we integrated the displacement profile over the intensity profile of the probe laser to obtain $\bar{\mathcal{U}}_z(x_0,\tau)$—corresponding to having excitation and probe lasers centered at x_0. Finally, we varied $0 \leqslant x_0 \leqslant l$ and determined the magnitude of the displacement generated at each position.

The first step in the above-described numerical analyses provided the ac temperature modulation in the beam to within a factor of Λ. For the device described in Fig. 1, the geometry and material absorption coefficient gave a total absorbed power ΛP_A of approximately $0.15P_0$. For instance, at $P_0=2$ mW and $\omega=\Omega_1$, the ac temperature modulation in the device of Fig. 1 was estimated to be $\sim$2.5 K. Note that the *average* temperature increase of the device may be much higher (see below). This ac temperature rise produced a rms displacement of $\sim$1.25 nm—in general agreement with the experimentally observed 10 nm displacement. We stress that the calculation up to this point involved *no* free parameters. The calculated rms amplitudes plotted as dashed lines in Figs. 1(b) and 1(c) were multiplied by a scale factor to emphasize the agreement in the mode shapes between experiments and calculations.

Returning to the results shown in Fig. 2, both the displacement and the thermal shift in Ω_1 depend linearly upon the excitation power over a limited range. It is important to note that the dc component of P_0 causes an average temperature rise, in addition to the small temperature modulation incurred by the ac component. We speculate that the geometry and the elastic properties of the device are affected by this average temperature rise. More measurements are necessary to determine the magnitude of this temperature rise and thus resolve the physical origin of the amplitude enhancement and large frequency shift at higher excitation power.

The spatial resolution of a photothermal probe is ultimately limited by the spatial extent of the heat source, which is dictated by both the thermal diffusion length and the laser spot size. For the excitation of the first harmonic mode of a nanomechanical beam at a frequency of $\sim$60 MHz, a thermal diffusion length of $\sim$0.61 μm and an excitation spot size of $\sim$1.93 μm were shown to be sufficient. For probing of higher modes on such devices, or for exciting fundamental mode in smaller structures, the spot size can be further reduced through a higher numerical aperture objective, shorter wavelength, or through the incorporation of a near-field optical probe.

In summary, we have demonstrated reliable photothermal NEMS operation with very high temporal and spatial resolutions and developed a model explaining the basic operational principles.

This work was supported in part by the NSF through Grants Nos. ECS-0210752, ECS-0304446, CMS-448796 and CMS-0324416. The authors would like to thank T. Kouh, B. B. Goldberg, and M. S. Ünlü for many helpful discussions.

[1] M. L. Roukes, Phys. World **14**, 25 (2001); H. G. Craighead, Science **290**, 1532 (2000).
[2] K. L. Ekinci, X. M. H. Huang, and M. L. Roukes, Appl. Phys. Lett. **84**, 4469 (2004); B. Ilic, H. G. Craighead, S. Krylov, W. Senaratne, C. Ober, and P. Neuzil, J. Appl. Phys. **95**, 3694 (2004).
[3] M. D. LaHaye, O. Buu, B. Camarota, and K. C. Schwab, Science **304**, 74 (2004); R. Knobel and A. C. Cleland, Nature (London) **424**, 291 (2003).
[4] K. L. Ekinci, Small **1**, 786 (2005).
[5] A. N. Cleland and M. L. Roukes, Appl. Phys. Lett. **69**, 2653 (1996).
[6] T. Kouh, O. Basarir, and K. L. Ekinci, Appl. Phys. Lett. **87**, 113112 (2005).
[7] A. San Paulo, J. Bokor, R. T. Howe, R. He, P. Yang, D. Gao, C. Carraro, and R. Maboudian, Appl. Phys. Lett. **87**, 053111 (2005).
[8] L. M. Zhang, D. Walsh, D. Uttamchandani, and B. Culshaw, Sens. Actuators, A **29**, 73 (1991); M. Zalalutdinov, A. Olkhovets, A. Zehnder, B. Ilic, D. Czaplewski, H. G. Craighead, and J. M. Parpia, Appl. Phys. Lett. **78**, 3142 (2001).
[9] B. Ilic, S. Krylov, K. Aubin, R. Reichenbach, and H. G. Craighead, Appl. Phys. Lett. **86**, 193114 (2005).
[10] K. C. Neuman and S. M. Block, Rev. Sci. Instrum. **75**, 2787 (2004).
[11] T. W. Murray and O. Balogun, Appl. Phys. Lett. **85**, 2974 (2004).
[12] In a separate set of measurements, we determined the intrinsic Q's of similar NEMS in high vacuum and then exposed the resonators to air. The atmospheric damping caused the Q's to go down to $\sim 10^2$.
[13] A. N. Cleland, *Foundations of Nanomechanics* (Springer, New York, 2003).
[14] B. A. Boley and J. H. Weiner, *Theory of Thermal Stresses* (Dover, New York, 1997).
[15] K. E. Petersen and C. R. Giuarnieri, J. Appl. Phys. **50**, 6761 (1979).
[16] M. Necati Özışık, *Heat Conduction*, 2nd ed. (Wiley, New York, 1993).